Electronic Supplementary Material (ESI) for Sustainable Energy & Fuels.

Supporting Information

Effect of core engineering on triphenylamine derivative-based dopant-free hole-transporting materials for perovskite solar cells: from theoretical calculation to experimental research

Qian Chen, Puhang Cheng, Hongyuan Liu, Xiaorui Liu*

Key Laboratory of Luminescence Analysis and Molecular Sensing, Ministry of Education, School of Chemistry and Chemical Engineering, Southwest University, Chongqing 400715, P.R. China

*Corresponding authors: Xiaorui Liu; E-mail addresses: liuxiaorui@swu.edu.cn (X. Liu)

Contents:

1. Computational details

1.1 Geometry optimization and electronic properties

We optimize the ground-state (S_0) geometry of investigated compound X25 and CQ1-CQ3 using the B3P86/6-311G(d,p) method and basis set.[1] The energies of all of the obtained geometries are ensured to be the lowest because the optimized structures do not exhibit imaginary frequency. The vibrational analysis was also using the same theoretical level to guarantee that the optimized geometry (Fig. S1) was the minimum of potential energy surface. Moreover, energy calculations, including electron affinities, adiabatic ionization potential and absolute hardness of the investigated systems, were performed using the BMK/6-31G(d) method. The solvation free energy for all molecules was calculated using the TD-BMK/6-31G(d) method in chlorobenzene solution or in gas.

1.2 Calculations of optical absorption

The optical absorptions of X25 were simulated by TD-DFT with B3P86, B3LYP, PBE0 and BMK at 6-31G(d) level in dichloromethane solution with a polarizable continuum model (PCM).[2] The maximum absorption of X25 for B3P86, B3LYP, PBE0 and BMK methods are 370, 369, 352 and 328 nm, respectively. The calculated result shows that maximum absorption wavelength ($\lambda_{abs,cal}$) of X25 (328 nm) from the TD-BMK/6-31G(d) calculations is in line with that of experimental value (335 nm).[3] Therefore, the optical properties of CQ1-CQ3 are calculated by TD-BMK/6-31G(d) functional and basis set in dichloromethane solution.

1.3 Calculations of charge mobility

The charge mobility of the designed HTMs was calculated from the Einstein relation:[4]

$$\mu = \frac{eW}{k_B T} \tag{S1}$$

Where e is the electron charge and W is the charge diffusion coefficient. k_B and T is the Boltzmann constant and temperature in Kelvin, respectively For a n-dimensional system, W is defined as the ratio between the mean-square displacement and the diffusion time:[5]

$$W = \lim_{t\to\infty} \frac{1}{2n} \frac{\left\langle x(t)^2 \right\rangle}{t} \quad \text{(S2)}$$

For a spatially isotropic system, the homogeneous diffusion constant W can be approximately evaluated by:[4]

$$W = \frac{1}{2n} \sum_i r_i^2 k_i p_i \quad \text{(S3)}$$

where n is the spatial dimensionality, i runs over all nearest adjacent molecules. and r_i, k_i and p_i are the corresponding center-to-center hopping distance, charge transfer rate (k), and hopping probability ($p_i = k_i / \sum_i k_i$), respectively.

Here, the parameter of charge transfer rate (k) for organic molecules can be calculated from the Marcus–Hush equation:[6]

$$k = \frac{\nu^2}{h} \sqrt{\frac{4\pi^3}{\lambda k_B T}} \exp\left(\frac{-\lambda}{4 k_B T}\right) \quad \text{(S4)}$$

Where h, v and λ are the Planck's constant, electronic coupling, reorganization energy [7], respectively. T is the temperature (in this calculation is set to 300 K). It's reported that descriptions of the charge transfer on basis of the hopping mechanism was universally accepted. In equation (S4), the parameters such as λ and v are the key factors to determine the transfer rate of organic materials.

In equation (S1), for an optimal transport system, electronic coupling should be maximized and λ should be minimized.

The inner reorganization energy λ_h for holes of HTMs could be calculated as follows:

$$\lambda_h = E_+ - E_+^* + E^* - E \quad \text{(S5)}$$

where E represent the total energy of the neutral segment and E_+^* is the cation segment. E_+ represent the energy of the neutral segment from the geometries of cation segment. E^* is the cation segment on basis of the neutral segment.[8] Energies of the neutral segment and the cation segment for inner reorganization energy of HTMs were performed using the LC-wPBE/6-311G(d,p) method and basis set.

The parameter of electronic coupling (v) could be obtained from the equation as shown below:[9]

$$v = \frac{J - S(H_1 + H_2)/2}{1 - S^2} \quad \text{(S6)}$$

where S, J and H are the spatial overlap, charge transfer integral and site energies. The parameter of J could be simulated by the equation as shown below:[9]

$$J = \left\langle \varphi^1_{\mathrm{HOMO}} \middle| h_{\mathrm{ks}} \middle| \varphi^2_{\mathrm{HOMO}} \right\rangle \quad \text{(S7)}$$

where h_{ks} is the Kohn-Sham Hamiltonian between two fragments. The parameters such as $\varphi^1{}_{\mathrm{HOMO}}$ and $\varphi^2{}_{\mathrm{HOMO}}$ are the HOMOs of two fragments, respectively. The electronic coupling could be simulated from the PW91/TZP levels in ADF program.[10-13]

The DFT and TD-DFT calculations were carried out by the Gaussian 09 program.[14]

1.4 Simulation of crystal structures

In order to calculate the parameter of electronic coupling for HTMs, it was compelled to obtain the dimer structure, which was defined as adjacent segments from the crystal structures of molecules. The crystal structure of the investigated HTMs can be predicted from the polymorph module in Material Studio software.[9] The geometry of the cluster models used in the present study was taken from the B3P86/6-311G(d,p) level. The Deriding force field was used for the prediction.[15]

For the investigated molecules, the polymorph calculations are restricted to the six most probable space groups such as $P2_1/c$, $P1$, $P2_12_12_1$, $C2/c$, $P2_1$ and $Pbca$.[16] Then, the crystal structures were sorted according to their total energy. On basis of the crystal structures, we selected a molecule as center. All of the adjacent fragments with the center are defined as the transport pathways. That is to say, each transport pathway is the paired dimer between neighboring and center molecules.

2. Experimental section

2.1 Materials

All starting reagents and solvents were used as received from commercial sources and used as received unless specially stated. Including 2,8-dibromo dibenzo [b, d] thiophene, 3,6-dibromo-9-(4-methoxyphenyl)-9H-carbazole, 4-methoxy-N-(4-methoxyphenyl)-N-(4-(4,4,5,5-tetramethyl-1,3,2-dioxaborolan-2-yl) phenyl) aniline. PEDOT:PSS (Heraeus, Clevios PVP Al 4083), PbI_2 (*p*-OLED, >99.99%), $PbCl_2$ (*p*-OLED, >99.99%), MAI (*p*-OLED, ≥99.5%), C60 (*p*-OLED, >99.5%), Spiro-OMeTAD (*p*-OLED, ≥99.5%), MoO_3 (Sigma-Aldrich, 99.97%), DMF (Sigma-Aldrich, 99.8%), DMSO (Sigma-Aldrich, 99.8%) and CB (Sigma-Aldrich, 99.8%). The SnO_2 solution was purchased from Alfa Aesar (tin (IV) oxide, 15 wt% in H_2O colloidal dispersion).Solvents for chemical synthesis such as THF, DMF, DMSO, CB, DCM and toluene were treated according to the standard procedures.

2.2 Device fabrication

Patterned ITO glass was cleaned in an ultrasonic bath in detergent, deionized water, acetone, isopropanol sequentially and then treated with a plasma for 3 min. Sonicate the prepared SnO_2 solution for 30 minutes. Spin-coating at 5000 rpm for 30 s to prepare SnO_2 film. After that, the

deposited SnO_2 film was annealed on a hot plate at 170 °C for 1 hour. Then the samples were transferred into a N_2-filled glovebox. The electron transporting layer C_{60} (5mg/mL) was deposited by spin-coating (5000 rpm for 30 s) corresponding solution on top of SnO_2 film. A perovskite precursor solution (1.26 M PbI_2, 0.14 M $PbCl_2$ and 1.4 M MAI in DMF:DMSO mixed solution with a v/v of 4:1) was spin-coated in a two-step program at 400 and 4000 rpm for 3 and 30 s, respectively. During the second step, 200 μL of chlorobenzene was dropped on the spinning substrate at 10 s after the start-up. Next, the as-spun perovskite layer was annealed on a hot plate at 60 °C for 1 min and at 85 °C for 25 min to drive off solvent and form the perovskite phase. The hole-transporting layers (HTLs) were deposited by spin-coating (4000 rpm for 30 s) corresponding solution on top of perovskite films. Different HTMs were all dissolved in CB. Afterwards, 7 nm thick MoO_3 was then thermally evaporated, and an approximately 100 nm thick Ag counter electrode was deposited on top to finish the device fabrication. The active area of our device is 0.06 cm^2.

2.3 The space-charge-limited current (SCLC) hole mobility measurements

Hole-only devices are fabricated with the structure ITO/PEDOT:PSS/HTM/MoO_3(7 nm)/Ag (100 nm). The dark *J–V* characteristics of hole-only devices were measured under N_2 atmosphere inside a glove box. PEDOT:PSS was deposited on the ITO substrate at 5000 rpm for 30 s, followed by annealing at 120 ºC for 30 min and the conditions of spin coating HTM are consistent with the Device fabrication. Mobility is extracted by fitting the current density-voltage curves using space charge limited current (SCLC). Fitting the results to a space charge limited form, based on the following equation $J = 9\varepsilon_\theta\varepsilon_\gamma\mu_h V^2/8L^3$. J is the current density, L is the film thickness of the active layer, μ_h is the hole mobility, ε_γ is the relative dielectric constant of the transport medium, ε_θ is the

permittivity of free space (8.85×10^{-12} F m^{-1}), V is the internal voltage of the device.

2.4 Measurements

The nuclear magnetic resonance (NMR) spectra were obtained from a BRUKER AVANCE Ⅲ 600 MHz NMR Instrument (in $CDCl_3$ or in DMSO). Mass spectra were collected on a Bruker impact II high-resolution mass spectrometer. UV-vis absorption spectra were measured on a Shimadzu UV-2450 absorption spectrophotometer. Cyclic voltammetry studies were conducted using a CHI660E system in a typical three-electrode cell with a glass carbon working electrode, a platinum wire counter electrode, and a silver/silver chloride (Ag/AgCl) reference electrode. All electrochemical experiments were carried out under a nitrogen atmosphere at room temperature in an electrolyte solution of 0.1 M tetrabutylammonium hexa-fluorophosphate (Bu_4NPF_6) in acetonitrile at a sweeping rate of 100 mV s^{-1}. The potential of Ag/AgCl reference electrode was internally calibrated by using the ferrocene/ferrocenium redox couple (Fc/Fc^+). According to the onset oxidation potential of the CV measurements, the highest occupied molecular orbital (HOMO) of CQ2 was estimated. The HOMO energy levels of X25 from the reference.[3] Since the oxidation potential of CQ2 is 0.07 eV larger than X25, the HOMO energy level of CQ2 is calculated to be 5.29 eV. The cross-sectional SEM image of the device was characterized by FE-SEM images (JEOL-880F). Use atomic force microscopy (AFM) to characterize the morphology, the model is CSPM5500A. Steady-state PL spectra were recorded on Fluorolog®-3 fluorescence spectrometer (Horiba). Time-resolved PL decay curves were measured by a single photon counting spectrometer from Horiba Instruments (Fluorolog®-3) with a Picosecond Pulsed UV-LASTER (LASTER375) as the excitation source. The current–voltage (J–V) curves were measured under 100 mW cm^{-2} (AM 1.5

G) simulated sunlight using Keithley 2400 in conjunction with a Newport solar simulator (94043A). Film thickness of hole transport layer and perovskite layer were measured by Surfcorder ET150, Kosaka Laboratory Ltd. The external quantum efficiency (EQE) was calculated from the photocurrent measurement under monochromatic illuminations at different wavelengths, using a 150 W xenon lamp and a monochromator.

3. Target molecule synthesis

The parent molecule X25 was synthesized through the Suzuki cross coupling reaction. Refer to this article for the specific synthesis route.[17] The characterization data are as follows:

4,4'-(9-(4-methoxyphenyl)-9H-carbazole-3,6-diyl)bis(N,N-bis(4-methoxyphenyl)-aniline) (X25): ^{1}H NMR (600 MHz, DMSO-d_6) δ 8.57 (s, 2H), 7.67 (s, 2H), 7.62 (s, 4H), 7.56 (s, 2H), 7.33 (d, J = 8.6 Hz, 2H), 7.23 (d, J = 8.8 Hz, 2H), 7.05 (d, J = 8.8 Hz, 8H), 6.97 – 6.88 (m, 12H), 3.89 (s, 3H), 3.75 (s, 12H).

Synthesis of 4,4'-(dibenzo[b,d]thiophene-2,8-diyl)bis(N,N-bis(4-methoxyphenyl)-aniline) (CQ2): The compound 1 (0.171 g, 0.5 mmol) and the compound 2 (0.570 g, 1.32 mmol) were accurately weighed and put into the reaction flask, the catalyst $Pd(PPh_3)_4$ (0.057 g, 0.05 mmol) was added under a nitrogen atmosphere, the system was vacuum replaced three times, and the toluene (30 mL) and potassium carbonate solution(2M 15 ml) prepared by deoxygenation in advance were added. The reaction was refluxed at 110 ˚C overnight. Cool to room temperature, quench the reaction with water, dry with anhydrous sodium sulfate and extract the organic solvent with dichloromethane. The product was obtained by column chromatography (PE/EA = 5:1) as a white powder (0.380 g, yield: 82%).^{1}H NMR (600 MHz, Chloroform-d) δ 8.24 (s, 2H), 7.78 (d, J = 8.3

Hz, 2H), 7.57 (d, *J* = 8.1 Hz, 2H), 7.46 (d, *J* = 7.4 Hz, 5H), 7.00 (s, 8H), 6.94 (s, 4H), 6.78 (d, *J* = 8.4 Hz, 8H), 3.74 (s, 12H). ^{13}C NMR (151 MHz, $CDCl_3$) δ 155.97, 148.21, 140.97, 138.24, 137.68, 136.20, 133.12, 127.77, 126.59, 125.78, 123.03, 121.02, 119.35,114.79, 55.53. MS: m/z= 790.2867, calcd for $C_{52}H_{42}N_2O_4S$: 790.29.

4. Experimental characterization

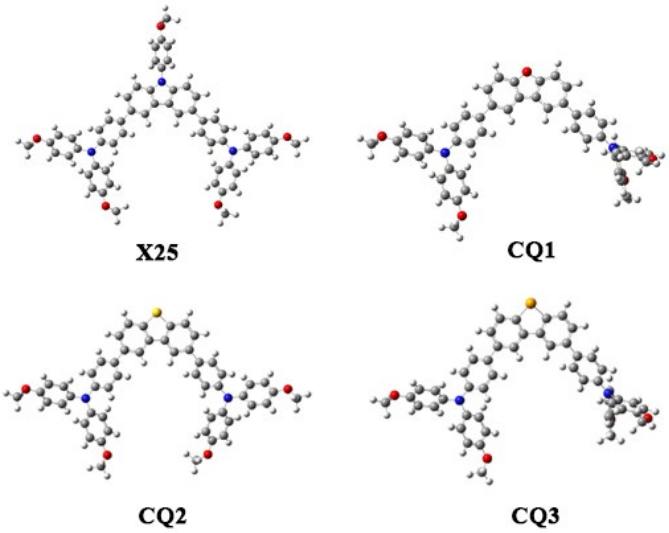

Fig. S1. Optimized geometries of the investigated molecules in this work as obtained using the B3P86/6-311G(d,p) method.

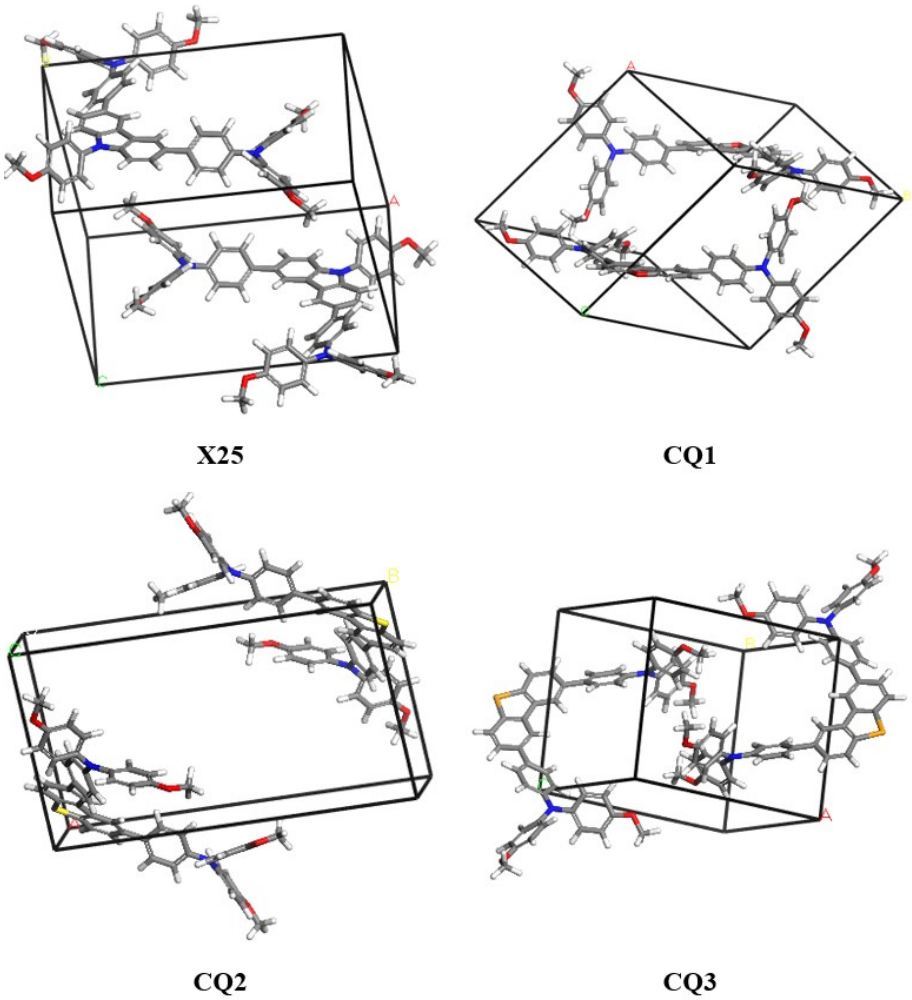

Fig. S2. Calculated crystal structures with the lowest total energies of the investigated molecules.

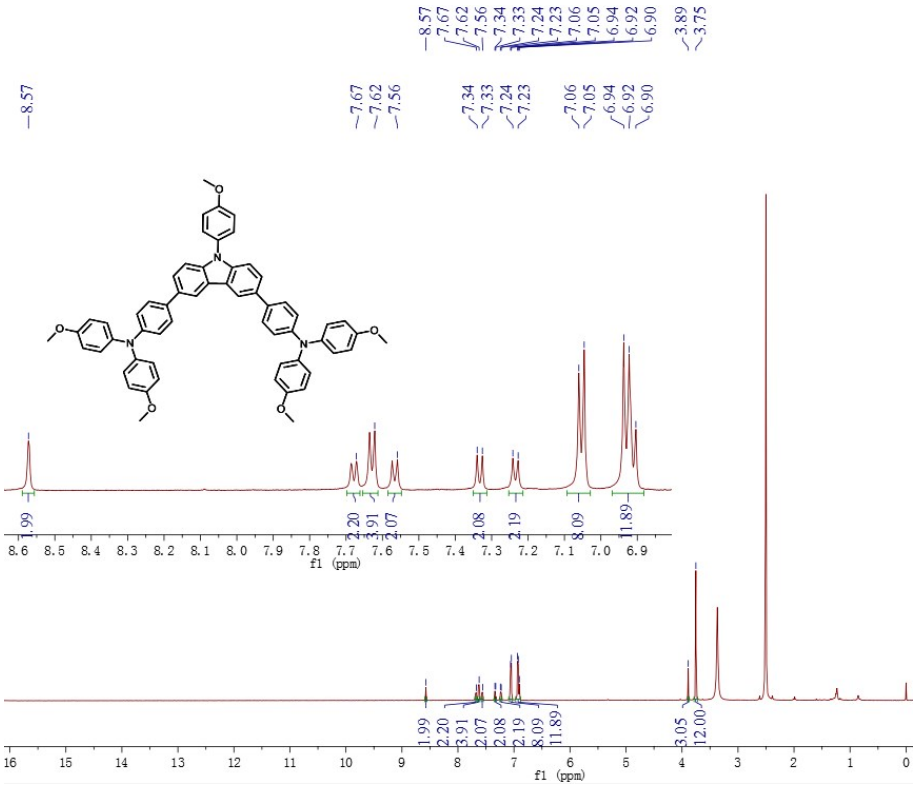

Fig. S3. The ^{1}H NMR spectrum of X25.

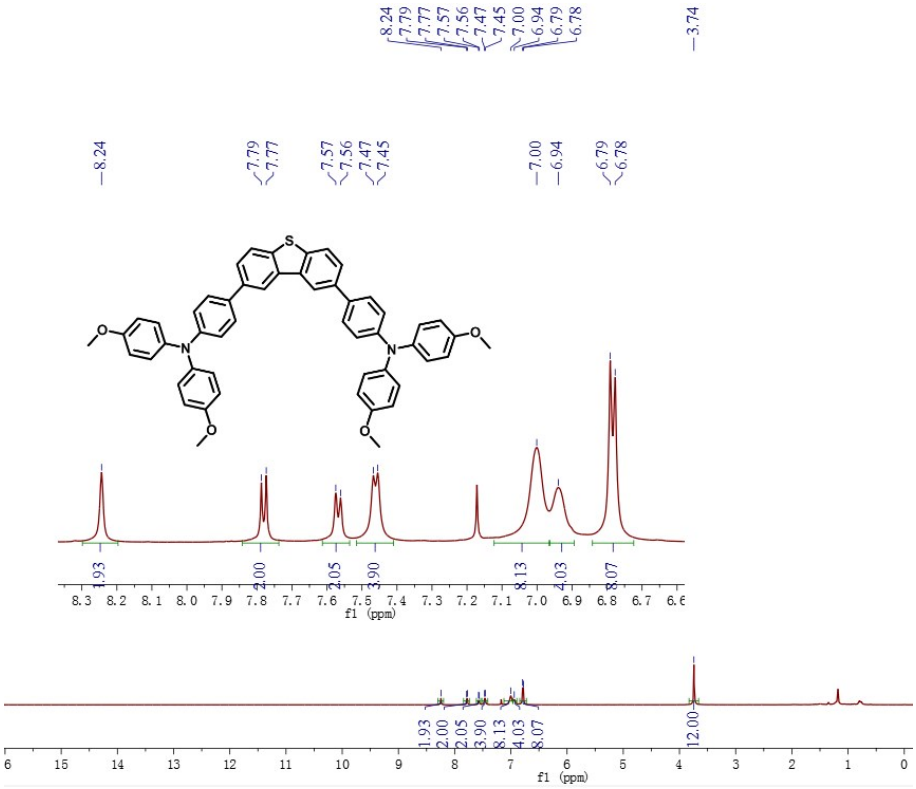

Fig. S4. The ^{1}H NMR spectrum of CQ2.

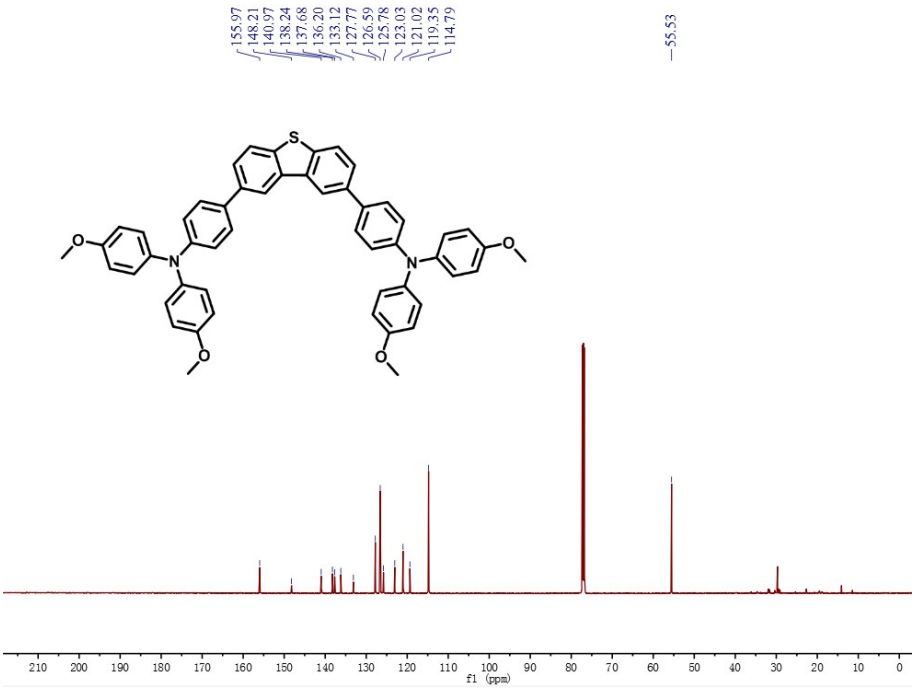

Fig. S5. The ^{13}C NMR spectrum of CQ2.

MASS SPECTROMETRY REPORT

Sample No.	Formula (M)	Measured m/z	Calc. m/z	Diff (ppm)
CQ2	$C_{52}H_{42}N_2O_4S$	790.2867	790.29	-0.9

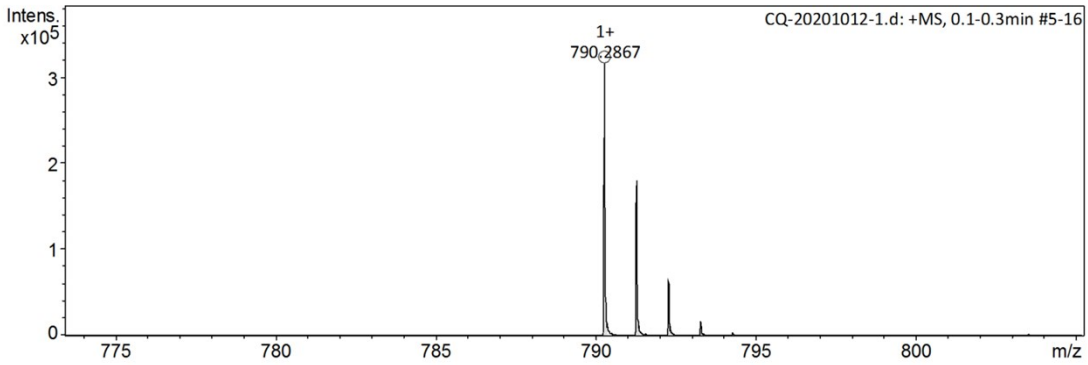

Fig. S6. Mass spectrometry of CQ2.

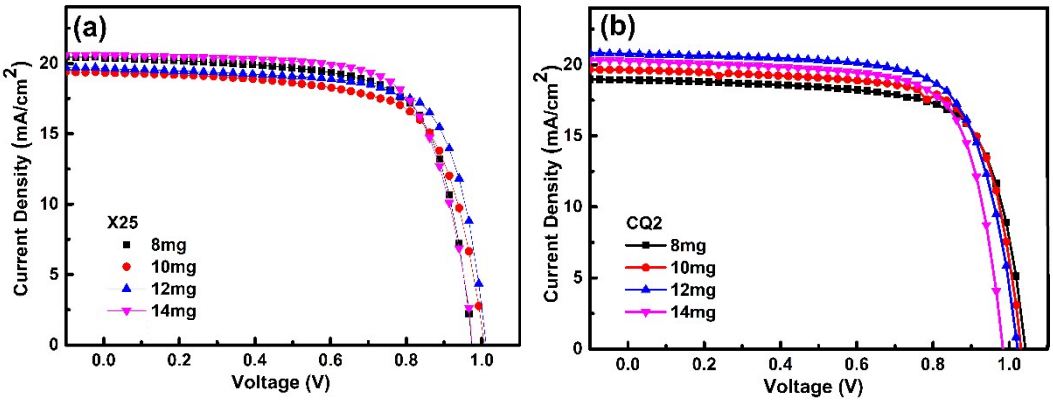

Fig. S7. Photovoltaic performance of PSCs with the HTMs X25(a) and CQ2(b), measured at different HTM concentrations.

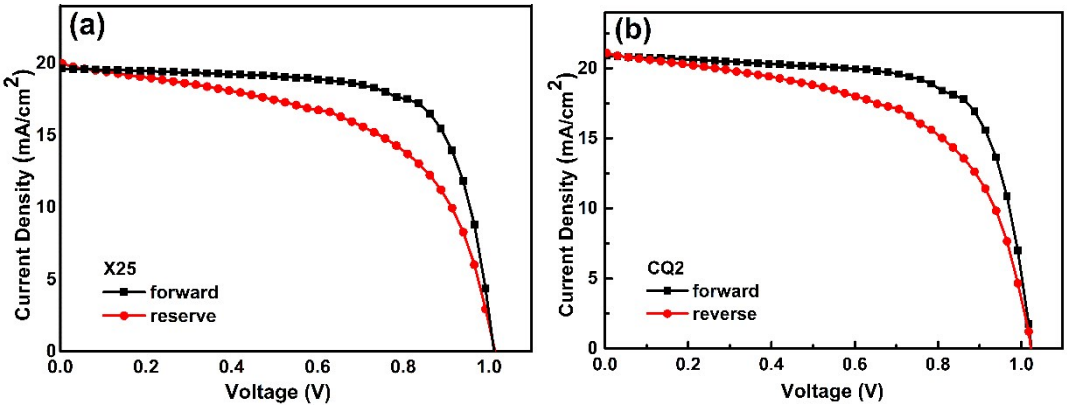

Fig. S8. *J–V* curves measured under reverse and forward voltage scans with X25(a) or CQ2(b) as HTMs.

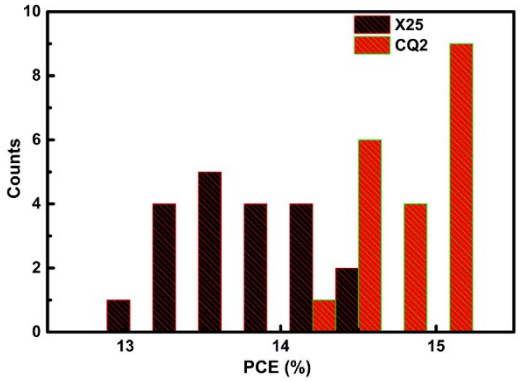

Fig. S9. Inset diagram: histogram of devices efficiencies based on X25 and CQ2.

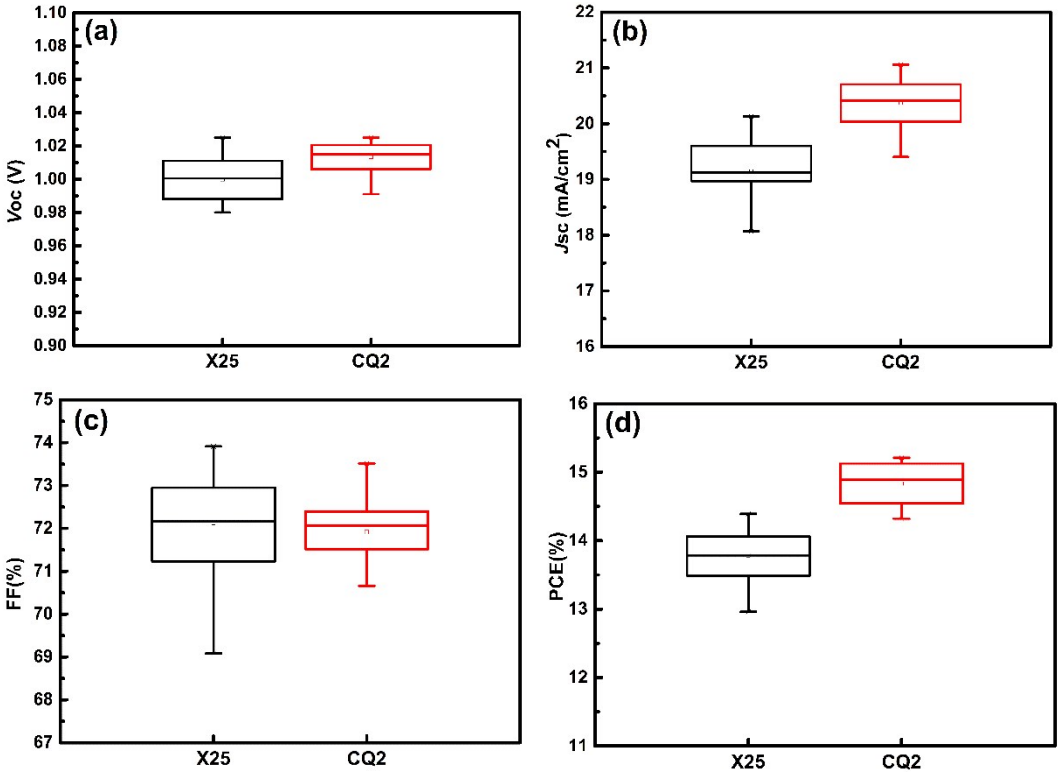

Fig. S10. Box charts of the photovoltaic parameters of X25 and CQ2.

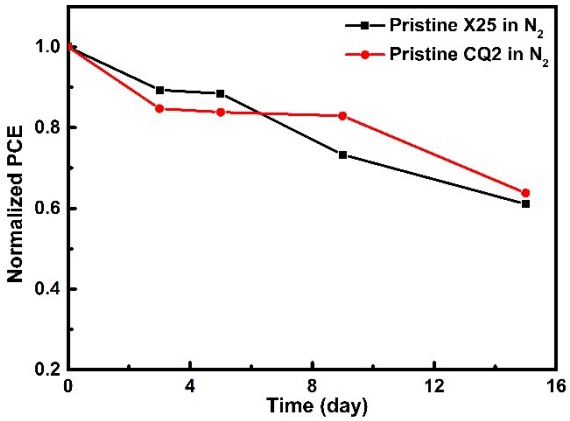

Fig. S11. Stability test of PSCs based on X25 and CQ2 HTMs under room temperature in the dark. The solar cells are stored in a box with a relative humidity of 10% filled with the N_2 gas.

Table S1. HOMO, LUMO and energy gap of X25 and CQ1-CQ3 from theoretical calculations.

	X25(exp.)[a]	X25[b]	CQ1[b]	CQ2[b]	CQ3[b]
HOMO/eV	-5.22	-5.20	-5.31	-5.32	-5.31
LUMO/eV	-1.99	-2.11	-2.26	-2.25	-2.26
E_g/eV	3.23	3.09	3.05	3.07	3.05

[a] from ref.[3]

[b]The HOMO and LUMO energy calculated by B3P86/6-311G(d,p) is fitted according to the formula:[1]

HOMO(exp) = 0.66 HOMO (th.) -1.75 (R=0.79)

LUMO(exp) = 0.69 LUMO (th.) -1.07 (R=0.88)

Table S2. Photovoltaic parameters for the PSCs devices based on studied HTMs with different concentrations.

HTM	Concentrations	V_{oc} [V]	J_{sc} [mA cm^2]	*FF* [%]	PCE [%]
X25	14 mg/mL	0.974	20.58	70.17	14.22
	12 mg/mL	1.012	19.64	72.42	14.39
	10 mg/mL	1.007	19.33	69.01	13.43
	8 mg/mL	0.973	20.39	70.28	13.95
CQ2	14 mg/mL	0.983	20.26	72.19	14.38
	12 mg/mL	1.018	20.57	72.65	15.21
	10 mg/mL	1.031	19.62	72.29	14.62
	8 mg/mL	1.042	18.91	72.41	14.28

Table S3. Summary of hysteresis index (HI) and device performance of perovskite solar cell adopting different hole transporting materials at forward and reverse voltage scans.

HTM		V_{oc} [V]	J_{sc} [mA cm^2]	*FF* [%]	PCE [%]	HI [%]
X25	forward	1.012	19.64	72.42	14.39	22.2
	reverse	1.014	20.00	55.25	11.20	
CQ2	forward	1.012	20.58	72.65	15.21	16.5
	reverse	1.021	20.80	59.80	12.70	

5. References

1. X. R. Liu and X. Liu, *RSC Adv.*, 2019, **9**, 24733-24741.
2. J. Tomasi, B. Mennucci and R. Cammi, *Chem. Rev.*, 2005, **105**, 2999-3094.
3. L. Y. Liu, Y. G. Wu, M. Y. Li, X. P. Zong, Z. Sun, M. Liang and S. Xue, *Chem. Commun.*, 2018, **54**, 14025-14028.
4. W. Q. Deng and W. A. Goddard, *J. Phys. Chem. B.*, 2004, **108**, 8614-8621.
5. J. Bisquert, *Phys. Chem. Chem. Phys.*, 2008, **10**, 3175-3194.
6. R. A. Marcus, *Annu. Rev. Phys. Chem.*, 1964, **15**, 155-196.
7. V. Coropceanu, J. Cornil, D. A. da Silva Filho, Y. Olivier, R. Silbey and J.-L. Brédas, *Chem. Rev.*, 2007, **107**, 926-952.
8. B. C. Lin, C. P. Cheng and Z. P. M. Lao, *J. Phys. Chem. A.*, 2003, **107**, 5241-5251.
9. K. Senthilkumar, F. Grozema, F. Bickelhaupt and L. Siebbeles, *J. Chem. Phys.*, 2003, **119**, 9809-9817.
10. ADF2014 SCM Theoretical Chemistry, Vrije Universiteit, Amsterdam, The Netherlands, http://www.scm.com.
11. G. te Velde, F. M. Bickelhaupt, E. J. Baerends, C. Fonseca Guerra, S. J. A. van Gisbergen, J. G. Snijders and T. Ziegler, *J. Comput. Chem.*, 2001., **22**, 931-967.
12. J. P. Perdew, J. A. Chevary, S. H. Vosko, K. A. Jackson, M. R. Pederson, D. J. Singh and C. Fiolhais, *Phys Rev B Condens Matter.*, 1992, **46**, 6671-6687.
13. C. Fonseca Guerra, J. G. Snijders, G. te Velde and E. J. Baerends, *Theor. Chem. Acc.*, 1998, **99**, 391-403.
14. M. J. Frisch, G. W. Trucks, H. B. Schlegel, G. E. Scuseria, M. A. Robb, J. R. Cheeseman, G. Scalmani, V. Barone and G. A. Petersson, *Fox, "Gaussian 09," Revision A.1, Gaussian, Inc., Wallingford, 2009.*
15. R. F. Jin and Y. F. Chang, *Phys. Chem. Chem. Phys.*, 2015, **17**, 2094-2103.
16. W.-J. Chi and Z.-S. Li, *Phys. Chem. Chem. Phys.*, 2015, **17**, 5991-5998.
17. J. B. Zhang, B. Xu, M. B. Johansson, N. Vlachopoulos, G. Boschloo, L. Sun, E. M. J. Johansson and A. Hagfeldt, *ACS Nano.*, 2016, **10**, 6816-6825.